INSTITUTE OF PHYSICS PUBLISHING JOURNAL OF PHYSICS B: ATOMIC, MOLECULAR AND OPTICAL PHYSICS

J. Phys. B: At. Mol. Opt. Phys. **35** (2002) 3041–3054 PII: S0953-4075(02)33219-X

Resonance energies, oscillator strengths and autoionization widths of the 1s–2p excitations from O IV low-lying states

Jiaolong Zeng and Jianmin Yuan

Department of Applied Physics, National University of Defense Technology, Changsha 410073, People's Republic of China

Received 31 January 2002, in final form 21 May 2002
Published 3 July 2002
Online at stacks.iop.org/JPhysB/35/3041

Abstract

The excitation energies and oscillator strengths of the 1s–2p transitions from O IV low-lying terms belonging to the configurations $2s^22p$, $2s2p^2$ and $2p^3$ are calculated using configuration interaction (CI) wavefunctions. Reasonably good agreement is obtained between the length and velocity forms. To verify the correctness of the results, these data are further obtained by treating the 1s–2p excitations as resonances occurring in photoionization processes. The photoionization cross sections are computed using the close-coupling scheme implemented by the *R*-matrix method. The resonance energies and autoionization widths of the 1s–2p excited states are determined by analysing the resonances exhibited by the photoionization cross sections. The results show that the resonance energies obtained by the *R*-matrix method are systematically lower than those by the CI scheme by 0.1–0.2 Ryd. This shows that a strong CI effect exists between the K-shell excited and continuum states. This effect can also produce redistribution of the oscillator strengths, especially for the weak transitions.

1. Introduction

Oxygen is an important element because of its existence in the Earth's atmosphere as well as in many astrophysical, laboratory spectra and diagnostic applications. O III and O IV are two of the most important ions in gaseous nebulae and other astrophysical objects. Fernley *et al* [1] calculated the energy levels, oscillator strengths and photoionization cross sections for the boron-like isoelectronic sequence including O IV ions. Their work was part of the Opacity Project (OP) [2, 3]. The OP used the close-coupling approximation to calculate energies and wavefunctions for bound states, oscillator strengths, photoionization cross sections and parameters for line broadening by electron impact. The computations were made using the *R*-matrix method [4]. Nahar [5] also calculated these radiative data including photoionization cross sections and oscillator strengths for O I–O VII ions for the analysis of astrophysical

and laboratory spectra using the R-matrix method. The calculations were carried out using eigenfunction expansions including $n = 3$ states. Recently, Tachiev and Froese Fischer [6] reported the Breit–Pauli results for energy levels, lifetimes and some transition data for all levels up to $2s2p(^3P)3s\ ^2P^o_J$ of the boron-like spectrum including O IV ions. However, all these researches were limited to valence-shell excitation or photoionization. There are no theoretical investigations, to the best of our knowledge, either on oscillator strengths of the K-shell transitions or on the autoionization widths of the K-shell excited states in the literature, although there have been some theoretical [7–9] and experimental [10] researches for atomic oxygen.

However, transition energies, oscillator strengths and the autoionization widths of the inner-shell transitions are important atomic data in dealing with inner-shell absorption or emission spectra. More and more efforts have been devoted to these inner-shell physical processes. Recently, x-ray photoabsorption in KLL resonances of O VI was predicted [11] and detected by the *Chandra X-ray Observatory* [12]. To analyse these K-shell resonances, one needs radiative data on the K-shell transitions.

During the past two decades, for theoretical studies on the K-shell spectroscopy and opacity of the plasmas, most calculations had been carried out by treating the K-shell transitions as bound–bound ones and by considering only the Doppler broadening. Abdallah and Clark [13] and Iglesias *et al* [14] simulated the x-ray transmission through aluminium plasmas by using such a method. However, the excitation energies of the K-shell transitions are well above the single-electron ionization threshold and they should be treated as photoionization and photoexcitation processes. Practical simulations [15–17] have shown that better agreement can be obtained with the experiments in such a way. Besides, the results have also shown that autoionization resonance broadening has a large effect on the x-ray transmission.

In this paper, we calculate the resonance energies and oscillator strengths of the K-shell 1s–2p transitions from O IV low-lying states in two different ways to show the difference between the results obtained by the above-mentioned two methods. The first one treats the K-shell excited states as bound ones and the results are obtained using the configuration interaction (CI) scheme implemented by the CIV3 code [18]. The second one treats the 1s–2p excitations as resonances occurring in photoionization processes. The photoionization cross sections are obtained using the close-coupling scheme employing the R-matrix method [4]. From the photoionization cross section that relates bound and continuum absorption, we can determine the resonance energies, oscillator strengths and the autoionization widths of the 1s–2p excitations. From the comparison of the results obtained by the two methods, we can get a clear understanding of the difference between the two methods.

2. Theoretical methods

The method of calculating the transition energies and oscillator strengths using the general CI code CIV3 can be found elsewhere [18, 19]. We present the outline of this method in the following. LS coupling is assumed throughout the paper. The CI wavefunction takes the form

$$\Psi(LS) = \sum_{i=1}^{M} a_i \Phi_i(\alpha_i LS), \tag{1}$$

where each of the configuration state functions $\{\Phi_i\}$ is built from one-electron orbitals whose angular momenta are coupled, in a manner defined by $\{\alpha_i\}$, to form a total L and S common to all configurations in (1). The one-electron orbital from which the $\{\Phi_i\}$ is constructed takes the form

$$u_{nlm_l}(\vec{r}, m_s) = \frac{1}{r} P_{nl}(r) Y_l^{m_l}(\theta, \phi) \chi(m_s), \tag{2}$$

and the radial functions are written as sums of Slater-type orbitals

$$P_{nl}(r) = \sum C_{jnl} r^{I_{jnl}} \exp(-\zeta_{jnl} r), \tag{3}$$

where we require

$$\int_0^\infty P_{nl}(r) P_{n'l}(r)\,\mathrm{d}r = \delta_{nn'}; \qquad (l < n' \leqslant n) \tag{4}$$

so that the orbitals form an orthonormal set.

The parameters of the radial functions are determined variationally by minimizing specific eigenvalues of a LS-coupled Hamiltonian matrix. For the CI method, we include six real and four pseudo-orbitals (1s, 2s, 2p, 3s, 3p, 3d, $\overline{4s}$, $\overline{4p}$, $\overline{4d}$ and $\overline{4f}$) to calculate the excitation energies and oscillator strengths for the 1s–2p transitions of O IV. The pertinent parameters ξ_{jnl} and coefficients C_{jnl} for all orbitals are obtained by using the CIV3 computer code [18] and they are given in our previous paper [20].

The wavefunctions in the form (1) for the O IV ions are used to calculate the absorption oscillator strengths, in both length (f_l) and velocity (f_v) forms. For the transitions from an initial state Ψ_i to a final state Ψ_j

$$f_l = \frac{\Delta E}{3g_i}\left|\langle\Psi_i|\sum_{p=1}^{N}\vec{r}_p|\Psi_j\rangle\right|^2, \tag{5}$$

$$f_v = \frac{4}{3g_i\Delta E}\left|\langle\Psi_i|\sum_{p=1}^{N}\nabla_p|\Psi_j\rangle\right|^2 \tag{6}$$

where $\Delta E = E_j - E_i$, E_i and E_j are, respectively, the energies (in Ryd) of initial and final states and $g_i = (2L_i + 1)(2S_i + 1)$ is the statistical weight of the lower state.

On the other hand, the resonance oscillator strengths of the K-shell excitations can also be obtained from the photoionization cross sections. It is well known that the photoionization cross sections can be obtained from the differential oscillator strengths $\mathrm{d}f/\mathrm{d}\epsilon$

$$\sigma_{PI} = \frac{\pi h e^2}{mc}\frac{\mathrm{d}f}{\mathrm{d}\epsilon} = 4\pi^2\alpha a_0^2\frac{\mathrm{d}f}{\mathrm{d}\epsilon}, \tag{7}$$

where h is Planck's constant, e the electron charge, m the electron rest mass, c the speed of light in vacuum, α and a_0 the fine-structure constant and the Bohr radius, respectively. In the latter expression of equation (7), ϵ is in Ryd. The resonance oscillator strengths can be obtained from the photoionization cross sections σ_{PI}

$$\begin{aligned}\overline{f}^r(L_iS_i \to L_jS_j) &= \int_{\Delta E_r}\left(\frac{\mathrm{d}f(L_iS_i \to L_jS_j)}{\mathrm{d}\epsilon}\right)\mathrm{d}\epsilon \\ &= \left(\frac{1}{4\pi^2\alpha a_0^2}\right)\int_{\Delta E_r}\sigma_{PI}(\epsilon; L_iS_i \to L_jS_j)\,\mathrm{d}\epsilon,\end{aligned} \tag{8}$$

where L_i, S_i, L_j, S_j are total spin and orbital angular momenta of the initial bound level and the final continuum wavefunction, governed by the dipole selection rules. As the cross sections σ_{PI} are usually calculated in length and velocity forms, the corresponding resonance oscillator strengths are determined in length $\overline{f}_l^r$ and velocity $\overline{f}_v^r$ forms as well.

For this work, the photoionization cross sections are calculated by the close-coupling approximation employing the R-matrix method [4]. The R-matrix method for electron–atom and photon–atom interactions has been discussed in great detail by Burke *et al* [21]. It is very effective in considering the resonance structures, and especially, the autoionization resonance widths are naturally included in the calculations and can be determined [19,22]. In an R-matrix calculation, the wavefunction of the $N + 1$ electron system is given the form

$$\Psi_k(X_1, \ldots, X_{N+1}) = \hat{A} \sum_{ij} c_{ijk} \Phi_i(X_1, \ldots, X_N, \hat{\boldsymbol{r}}_{N+1}\sigma_{N+1}) u_{ij}(r_{N+1}) + \sum_j d_{jk} \phi_j(X_1, \ldots, X_{N+1}), \quad (9)$$

where $\hat{A}$ is the antisymmetrization operator to take the exchange effect between the target electrons and the free electron into account. X_i stands for the spatial ($\boldsymbol{r}_i$) and the spin (σ_i) coordinates of the ith electron. The functions $u_{ij}(r)$ under the first sum construct the basis sets for the continuum wavefunctions of the free electron, and Φ_i are the couplings between the target states and the angular and spin parts of the free electron. The correlation functions ϕ_j in the second sum are constructed by the square integrable orbitals to account for the correlation effects not adequately considered because of the cut-off in the first sum. The square integrable orbitals are cast as linear combinations of Slater-type orbitals (equation (3)).

For the calculations of the photoionization cross sections from the O IV low-lying states, six real and four pseudo-orbitals (1s, 2s, 2p, 3s, 3p, 3d, $\overline{4s}$, $\overline{4p}$, $\overline{4d}$ and $\overline{4f}$) are included in the wavefunction expansion of the target O V ions. The pertinent parameters ξ_{jnl} and coefficients C_{jnl} for all orbitals are obtained by using the CIV3 code [18] according to the following rules. The 1s and 2s orbitals are the Hartree–Fock orbitals for the O V ground state $2s^2\ {}^1S$ given by Clementi and Roetti [23], while the 2p, 3s, 3p and 3d orbitals are optimized on the $2s2p\ {}^1P^o$, $2s3s\ {}^1S$, $2s3p\ {}^3P^o$, and $2s3d\ {}^1D$ states, respectively, using the same 1s and 2s orbitals for each. The pseudo-orbitals $\overline{4s}$ and $\overline{4p}$ are obtained by optimizing on the $2p^2\ {}^1S$ and $2s2p\ {}^1P^o$ states, respectively, while $\overline{4d}$ and $\overline{4f}$ are on the 1s-hole states $1s2s^22p\ {}^1P^o$ and $1s2s2p^2\ {}^3D$. The resulting orbital parameters of the radial functions for O V ions are compiled in table 1. The appropriate R-matrix wavefunction expansions are performed by including 21 states of O V which are listed in table 2, in which our calculated energy levels and the corresponding observed values [24] wherever available are also given. It can easily be seen that our calculated energy levels agree well with the experimental values. The differences between the experimental and calculated values are a few thousandths of Ryd. The relative differences are $<0.5\%$, mostly within 0.2%. Fernley *et al* [1] used three alternative methods (cases A, B and C) of optimizing the radial function in O V. From the energies they gave, one can see that case C was the best. The results obtained by Fernley *et al* using optimizing method C are also listed in table 2. In their calculations of the photoionization cross sections, they included six lowest terms which were in the $n = 2$ complex as the target states. It can be seen that the same degree of agreement with the observed values is obtained for our calculated excitation energies as those obtained by Fernley *et al* [1], or even a little better. Of course, we can include more correlated orbitals to obtain a better agreement with the observed values, but this will result in too many configurations in the $N + 1$ electron system and make calculation difficult to control.

In running the R-matrix codes, the R-matrix boundary is chosen to be 10 au to ensure that the wavefunctions are completely wrapped within the R-matrix sphere. For each angular momentum, the continuum orbitals are expressed as a linear combination of 40 numerical basis functions. In order to take into account the resonances of the K-shell excited state, only one electron is fixed in the 1s orbital, the other electrons can freely be distributed among the included orbitals.

3. Results and discussions

Table 3 gives the transition energies and oscillator strengths of the K-shell 1s–2p transitions obtained using the CI scheme implemented by the CIV3 code [18]. Both the length and velocity forms of the oscillator strengths are given to access the quality of the wavefunctions.

Table 1. Orbital parameters of the radial functions of the target ion O V.

Orbital	C_{jnl}	I_{jnl}	ξ_{jnl}
2p	0.285 75	2	2.752 58
	0.188 52	2	4.488 97
	0.549 45	2	2.614 35
	0.002 48	2	12.520 90
3s	−0.064 82	1	7.660 58
	−0.056 40	1	8.450 99
	1.313 99	2	2.064 89
	−0.085 07	2	6.321 29
	−6.405 00	3	1.746 74
	4.566 94	3	1.728 62
3p	−0.637 43	2	4.250 51
	0.379 45	2	4.205 17
	−0.549 76	3	3.099 80
	1.295 60	3	1.702 27
3d	0.995 42	3	1.658 22
	0.010 87	3	4.604 59
$\overline{4s}$	−0.376 99	1	6.351 15
	1.126 07	2	3.143 05
	−3.556 27	3	2.735 01
	1.561 36	4	5.303 70
	1.582 95	4	1.971 69
$\overline{4p}$	0.343 54	2	16.799 48
	−0.409 93	2	15.967 78
	−6.803 97	3	2.988 09
	−0.734 50	3	1.523 24
	7.636 77	4	3.631 91
$\overline{4d}$	−2.905 52	3	3.680 44
	0.665 24	3	5.278 24
	0.615 28	4	1.903 70
	1.275 23	4	3.993 42
$\overline{4f}$	0.128 00	4	2.801 74
	0.896 50	4	4.471 03

From inspection of table 3, one can see that approximate LS coupling holds for all the initial terms of the transitions, but strong CI exists for some upper states. Where the upper states mix strongly, the admixtures among the main various possible coupling are given. Reasonably good agreement is found between the length and velocity forms of the oscillator strengths. The relative difference is $<10\%$ for most transitions.

To test the reliability of the results obtained by the CI scheme, the resonance oscillator strengths of the 1s–2p transitions of O IV ions are further obtained from photoionization cross sections. The cross sections are calculated using the R-matrix method [4]. To have a complete understanding of photoionization over the valence- and K-shell ionization thresholds, the photoionization cross sections are obtained from the first ionization threshold at 5.6828 Ryd (theoretical result) to the K-shell ionization thresholds for the ground state $2s^2 2p\ ^2P^o$ of O IV. The results are given in figure 1(a). The calculated first ionization threshold agrees rather well with the experimental value of 5.6875 Ryd. In the work of Nahar [5]

Table 2. Calculated non-relativistic and experimental energy levels (in Ryd) for the target O v ions relative to the ground state.

State	Expt [24]	Calc.	Expt − Calc.	Diff. (%)	Fernley *et al* [1]
$(1s^2)2s^2\ ^1S$	0.0	0.0	0.0	0.0	0.0
$2s2p\ ^3P^o$	0.7494	0.7458	0.0036	0.48	0.7476
$2s2p\ ^1P^o$	1.4471	1.4524	−0.0053	0.37	1.4592
$2p^2\ ^3P$	1.9478	1.9440	0.0038	0.20	1.9502
$2p^2\ ^1D$	2.1116	2.1123	−0.0007	0.04	2.1158
$2p^2\ ^1S$	2.6236	2.6312	−0.0076	0.29	2.6440
$2s3s\ ^3S$	4.9844	4.9750	0.0094	0.19	
$2s3s\ ^1S$	5.1147	5.1065	0.0082	0.16	
$2s3p\ ^1P^o$	5.2929	5.2820	0.0109	0.21	
$2s3p\ ^3P^o$	5.3116	5.3046	0.0070	0.22	
$2s3d\ ^3D$	5.4746	5.4727	0.0019	0.04	
$2s3d\ ^1D$	5.5826	5.5839	−0.0013	0.02	
$1s2s^22p\ ^3P^o$		40.4197			
$1s2s(^3S)2p^2(^3P)^5P$		40.5832			
$1s2s^22p\ ^1P^o$		40.7771			
$1s2s(^3S)2p^2(^1D)^3D$		41.3515			
$(-0.731s2s(^1S)2p^2(^3P)$ $+ 0.671s2s(^3S)2p^2(^3P))^3P$		41.3619			
$1s2s(^3S)2p^2(^1S)^3S$		41.7662			
$1s2s(^1S)2p^2(^1D)^1D$		41.8448			
$(-0.661s2s(^1S)2p^2(^3P)$ $- 0.721s2s(^3S)2p^2(^3P))^3P$		41.9298			
$1s2s(^1S)2p^2(^1S)^1S$		42.2615			

and OP [3], the corresponding results are 5.674 Ryd, coincidentally the same for the two calculations. The differences between the theoretical and experimental values are 0.0047 and 0.014 Ryd, respectively, for our results and theirs. The relative differences are 0.08 and 0.25%, respectively. Obviously, our calculated ionization threshold is in better agreement with the experiment than that obtained by Nahar and OP. The comparison of the theoretical ionization thresholds obtained by the *R*-matrix and CI methods with the experimental values is displayed in table 4. It can easily be seen that the energies of the ionization thresholds obtained by the *R*-matrix method are in better agreement with the experiment than those by the CI method.

In figure 1(a), only the length form is given because the relative differences between the length and velocity forms are <6%. One can easily see that the complex resonance structures of the cross sections exist in two energy regions: around the L-shell resonances at the photon energy region from the first ionization threshold to about 11 Ryd and around the K-shell at about 40–47 Ryd. The detailed structures of the cross sections around the L-shell resonances have been given and analysed by Nahar [5], therefore we do not repeat them here. Some structures originating from the two-electron excitations are still identifiable in the photon energy range of 9–11 Ryd. Good agreement is obtained between our results and those of Nahar [5]. For example, the background cross section is 1.18 Mb at a photon energy of 8 Ryd, in rather good agreement with the value of about 1.2 Mb obtained by Nahar [5].

Another striking feature of the cross sections shown in figure 1(a) is that broad and strong resonances exist at about 40 Ryd, which are well above the first ionization threshold 5.6875 Ryd and are also higher than the second ionization limit O VI $1s^22s\ ^2S$ located at 14.0569 Ryd and the third one O VII $1s^2\ ^1S$ located at 24.2056 Ryd. The second and third ionization limits are

Table 3. Oscillator strengths and resonance energies (Ryd) for dipole allowed K-shell 1s–2p transitions from the low-lying states of O IV. Where the states mix strongly, the admixtures among the main various possible couplings resulting from the CI calculations are given.

		CIV3			*R*-matrix			
No	Transition	f_l	f_v	ΔE	E_r	$\overline{f}_l^r$	$\overline{f}_v^r$	Γ_a (meV)
1	$2s^22p\ ^2P^o–1s2s^22p^2\ ^2D$	0.1345	0.1234	40.1739	39.9848	0.1370	0.1330	140.1
2	$2s^22p\ ^2P^o–1s2s^22p^2\ ^2P$	0.2432	0.2277	40.2145	40.0787	0.2528	0.2445	66.7
3	$2s^22p\ ^2P^o–1s2s^22p^2\ ^2S$	0.0274	0.0265	40.4257	40.2224	0.0273	0.0268	125.2
4	$2s2p^2\ ^4P–1s2s(^3S)2p^3(^2D^o)^4D^o$	0.1325	0.1255	40.1069	39.8891	0.1377	0.1328	80.3
5	$2s2p^2\ ^4P–(-0.721s2s(^1S) - 0.681s2s(^3S))2p^3(^4S^o)^4S^o$	0.1086	0.0995	40.0754	39.9247	0.1108	0.1069	19.0
6	$2s2p^2\ ^4P–1s2s(^3S)2p^3(^2P^o)^4P^o$	0.0776	0.0754	40.3819	40.1399	0.0794	0.0776	59.9
7	$2s2p^2\ ^4P–(-0.681s2s(^1S) + 0.711s2s(^3S))2p^3(^4S^o)^4S^o$	0.0020	0.0022	40.9920	40.6992	0.0033	0.0033	87.1
8	$2s2p^2\ ^2D–(-0.731s2s(^1S) - 0.671s2s(^3S))2p^3(^2D^o)^2D^o$	0.2240	0.2157	40.1017	39.9337	0.2187	0.2109	115.6
9	$2s2p^2\ ^2D–(0.731s2s(^1S) + 0.661s2s(^3S))2p^3(^2P^o)^2P^o$	0.0726	0.0679	40.3589	40.1867	0.0703	0.0688	99.3
10	$2s2p^2\ ^2D–(0.661s2s(^1S) + 0.721s2s(^3S))2p^3(^2D^o)^2D^o$	0.0204	0.0207	40.5019	40.2800	0.0306	0.0298	133.3
11	$2s2p^2\ ^2D–(0.731s2s(^3S) - 0.661s2s(^1S))2p^3(^2P^o)^2P^o$	0.0068	0.0070	40.7641	40.5411	0.0099	0.0098	112.9
12	$2s2p^2\ ^2S–(0.731s2s(^1S) + 0.661s2s(^3S))2p^3(^2P^o)^2P^o$	0.3013	0.2743	39.9652	39.8391	0.2985	0.2859	99.3
13	$2s2p^2\ ^2S–(0.731s2s(^3S) - 0.661s2s(^1S))2p^3(^2P^o)^2P^o$	0.0277	0.0281	40.3905	40.1935	0.0436	0.0420	112.9
14	$2s2p^2\ ^2P–(-0.731s2s(^1S) - 0.671s2s(^3S))2p^3(^2D^o)^2D^o$	0.0142	0.0115	39.5906	39.4393	0.0164	0.0156	115.6
15	$2s2p^2\ ^2P–(0.731s2s(^1S) + 0.661s2s(^3S))2p^3(^2P^o)^2P^o$	0.0084	0.0071	39.8655	39.6924	0.0972	0.0934	99.3
16	$2s2p^2\ ^2P–(0.661s2s(^1S) + 0.721s2s(^3S))2p^3(^2D^o)^2D^o$	0.1259	0.1137	39.9798	39.7857	0.1194	0.1167	133.3
17	$2s2p^2\ ^2P–(0.731s2s(^3S) - 0.661s2s(^1S))2p^3(^2P^o)^2P^o$	0.0728	0.0671	40.2708	40.0468	0.0691	0.0685	112.9
18	$2s2p^2\ ^2P–1s2s(^3S)2p^3(^4S^o)^2S^o$	0.1066	0.1003	40.2441	40.0993	0.1133	0.1090	28.6
19	$2p^3\ ^4S^o–1s2p^4\ ^4P$	0.2266	0.2165	40.1237	39.8926	0.2260	0.2219	73.5
20	$2p^3\ ^2D^o–1s2p^4\ ^2D$	0.1141	0.1090	40.1958	39.9997	0.1143	0.1122	119.7
21	$2p^3\ ^2D^o–1s2p^4\ ^2P$	0.1157	0.1104	40.2811	40.1138	0.1189	0.1169	76.2
22	$2p^3\ ^2P^o–1s2p^4\ ^2D$	0.0689	0.0673	39.9174	39.6847	0.0701	0.0678	121.1
23	$2p^3\ ^2P^o–1s2p^4\ ^2P$	0.1257	0.1155	40.0001	39.7989	0.1309	0.1268	76.2
24	$2p^3\ ^2P^o–1s2p^4\ ^2S$	0.0499	0.0474	40.5011	40.2148	0.0491	0.0481	78.9

shown in figure 1(a) by dashed vertical lines. To see these structures more clearly, they are redrawn in figure 1(b) on an expanded scale as a solid curve. It can be easily seen that three resonances exist in the photon energy region of 39.9–40.3 Ryd. These resonances are caused by the 1s–2p excited autoionization states $1s2s^22p^2\ ^2D$, ^2P and ^2S. The resonance energies and autoionization widths of these 1s–2p excited states can be obtained by analysing these resonances using the same method as in our previous paper [20]. From the photoionization cross sections, the resonance oscillator strengths can be determined by using equation (8). The

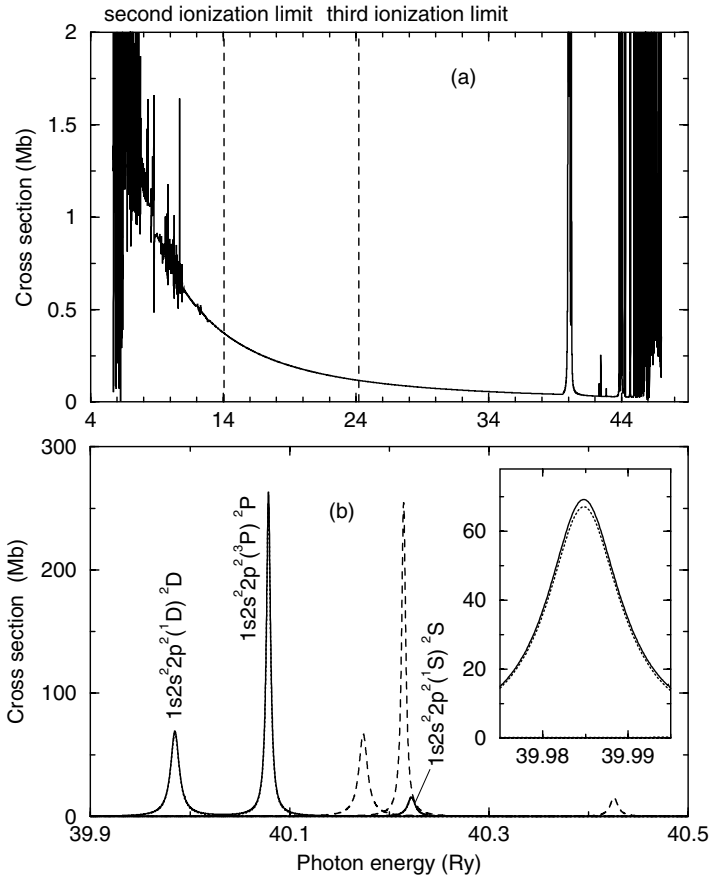

Figure 1. (a) Ground-state photoionization cross section of O IV from the first ionization threshold to the K-shell thresholds. The dashed vertical lines refer to the second (14.0569 Ryd) and third (24.2056 Ryd) ionization limits. (b) The 1s–2p resonances on an expanded scale. The solid curve refers to the result obtained by the *R*-matrix method, the dashed curve to the calculated photoabsorption cross section using the transition energies and oscillator strengths obtained by the CI scheme, and the dotted curve to the calculated photoabsorption cross section using the resonance energies obtained by the *R*-matrix method and oscillator strengths by the CI scheme. The inset is given to show the difference between the results shown by the solid and dashed curves.

final results are also displayed in table 3. For resonance oscillator strengths, both length and velocity forms are given for comparison.

The dashed and dotted curves in figure 1(b) refer to the photoabsorption cross section calculated from the following expression:

$$\sigma_{ij}(h\nu) = \frac{\pi h e^2}{mc} f_{ij} S(h\nu), \tag{10}$$

where $h\nu$ is the photon energy, and S is the line shape function which is assumed to be of Lorentzian profile

$$S(h\nu) = \frac{\Gamma/2\pi}{(h\nu - \Delta E)^2 + (\Gamma/2)^2} \tag{11}$$

where ΔE is the transition energy and Γ is the full-width of the line at half the maximum amplitude. The transition energy and oscillator strengths f_{ij} obtained by using the CI scheme

Table 4. Comparison of the present calculated energies obtained from the *R*-matrix (third column) and CI (fifth column) methods with the experimental values [24] and other theoretical results [3,5] (relative to the ground state of the target O ions). Energies are expressed in Rydberg units and negative signs are omitted for convenience.

State	Expt [24]	*R*-matrix	Diff. (%)	CI	Nahar [5]	OP [3]
$(1s^2)2s^2 2p\ ^2P^o$	5.6875	5.6828	0.08	5.6653	5.674	5.674
$2s2p^2\ ^4P$	5.0370	5.0388	0.04	5.0189	5.031	5.031
$2s2p^2\ ^2D$	4.5330	4.5260	0.15	4.4969	4.507	4.514
$2s2p^2\ ^2S$	4.1920	4.1783	0.33	4.1421	4.134	4.159
$2s2p^2\ ^2P$	4.0437	4.0317	0.03	3.9977	4.001	4.014
$2p^3\ ^4S^o$	3.5899	3.5822	0.21	3.5433	3.539	3.563
$2p^3\ ^2D^o$	3.3645	3.3606	0.12	3.3184	3.320	3.344
$2p^3\ ^2P^o$	3.0560	3.0456	0.34	2.9959	2.975	3.023

are used to derive the results shown by the dashed curve. Γ is taken to be the autoionization width of the corresponding upper state obtained by the *R*-matrix method. The dotted curve shown in figure 1(b) refers to the same results as the dashed curve except that the transition energy obtained by the *R*-matrix method is used. The solid and dotted curves are so close that one cannot see the differences clearly. To see the two curves clearly, we have redrawn the photoabsorption cross section around the $1s2s^22p^2\ ^2D$ resonance on an even more expanded scale in the inset shown in figure 1(b) and it can be seen that the maximum value shown by the dotted curve is a little smaller than that shown by the solid curve.

In figure 2 the solid curve displays the photoionization cross sections from the excited configuration $2s2p^2$ with (a) referring to ^4P, (b) to ^2D, (c) to ^2S, and (d) to the ^2P term. In figure 3 the solid curve shows the photoionization cross sections from the configuration $2p^3$ with (a) referring to $^4S^o$, (b) to $^2D^o$, and (c) to the $^2P^o$ term. The meaning of the dashed and dotted curves is the same as in figure 1(b). Table 4 shows the energies of these terms relative to the ground state of the target O V ions obtained by the *R*-matrix and CI methods. The experimental values and theoretical results obtained by Nahar [5] and OP [3] are also given for comparison. It can be seen that rather good agreement is found between our calculated energies obtained by the *R*-matrix method and the experiment. The relative differences are less than 0.34% for all the terms except the $2p^3\ ^2P^o$ term. Even for this term, our result is in better agreement with the experiment than the results obtained by Nahar [5] and OP [3]. The (relative) differences between the experimental and theoretical results obtained by Nahar [5] and OP [3] are 0.045 Ryd (2.65%) and 0.021 Ryd (1.08%), respectively, which are larger than our result 0.0104 Ryd (0.34%). The difference between the experimental and our theoretical results for the $2p^3\ ^2P^o$ term may partly be due to the omission of the correlation with the $2p^5\ ^2P^o$ term.

The resonance energies, oscillator strengths and autoionization widths are determined from figures 2 and 3 and the results are also given in table 3. For the resonance oscillator strengths, both the length and velocity forms are obtained from the length and velocity forms of corresponding photoionization cross sections. Table 3 is grouped according to the initial terms of the transitions. For the same initial terms, the transitions are arranged in the order of increasing resonance energies.

From inspection of the results shown in figures 1(b), 2, 3 and table 3, we can draw some conclusions. Firstly, the background cross sections are very small when away from resonances. Take the ground state $2s^22p\ ^2P^o$ of O IV as an example. Peaks occurred in the region from 39.9 to 40.3 Ryd for the 1s–2p resonances. The maximum cross sections for the three resonances

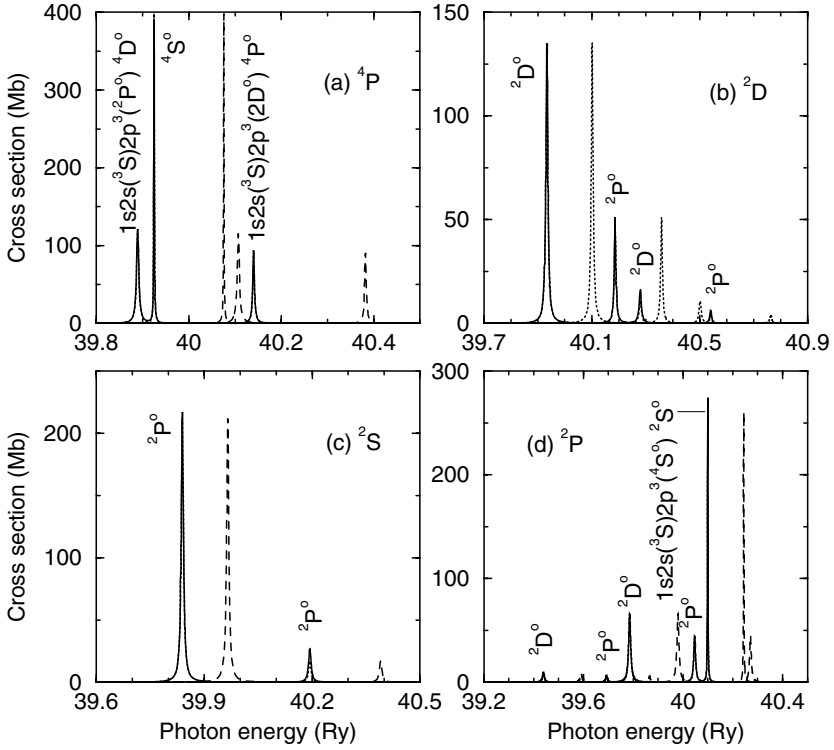

Figure 2. The photoionization cross sections of the configuration $2s2p^2$: (a) ^{4}P, (b) ^{2}D, (c) ^{2}S, and (d) ^{2}P in the vicinity of 1s–2p resonances. The meanings of the solid, dashed and dotted curves are the same as in figure 1(b).

$1s2s^22p^2$ ^{2}D, ^{2}P and ^{2}S which are located at 39.9848, 40.0787 and 40.2224 Ryd are about 69, 263, and 16 Mb, respectively, while for the cross section away from these resonances, the cross section is only 0.052 Mb at a photon energy of 35 Ryd, and it decreases to 0.042 Mb at a photon energy of 39 Ryd. Secondly, the resonance energies obtained by the *R*-matrix method are systematically lower than the transition energies obtained by the CI method by, typically, 0.1–0.2 Ryd. The main reason should be that strong interaction exists between the K-shell excited states and continuum states. As the CI method does not include this physical effect while the *R*-matrix method does, we believe that the results obtained by the *R*-matrix method should be more accurate. Present results show that the CI effects in the continuum are so large that omission of them will result in over-estimation of the transition energies. Such a conclusion can easily be drawn from table 5, which shows the energies of the lower and upper states of the 1s–2p transitions obtained by the *R*-matrix and CI methods. Note that the number of transitions is the same as in table 3. Thirdly, good agreement is found between the length and velocity forms of the resonance oscillator strengths obtained by the *R*-matrix method. The relative differences are $<5\%$ for all transitions concerned, most of which $<2\%$. The good agreement reflects the quality of the calculated photoionization cross sections. For the strong transitions, the length form of the oscillator strengths obtained by the CI method also agrees well with the results obtained by the *R*-matrix method. However, for the weak transitions whose oscillator strengths are small, some differences exist. The resonance oscillator strengths obtained by the *R*-matrix method are generally larger than the corresponding results obtained by the CI

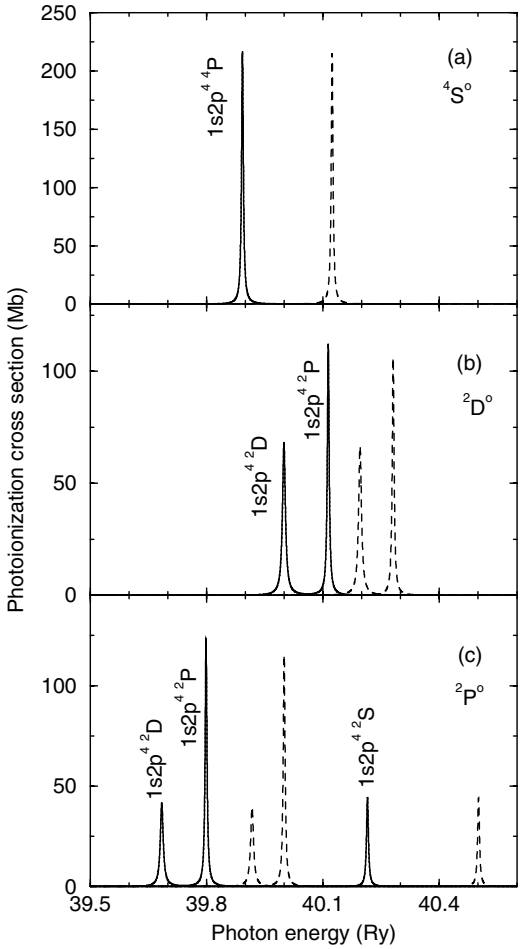

Figure 3. As figure 2, but for the configuration $2p^3$: (a) $^4S^o$, (b) $^2D^o$ and (c) $^2P^o$.

method. For example, for transition $2s2p^2\,^2D$–$(0.661s2s(^1S) + 0.721s2s(^3S))2p^3(^2D^o)^2D^o$, the length form of oscillator strengths obtained by the CI method is 0.0204, but the corresponding value by the *R*-matrix method is 0.0306, the latter being 50% larger than the former. The redistribution of these oscillator strengths should also be attributed to the CI effects between the K-shell excited states and continuum states. Finally, the CI effects with the continuum states are different for different states. An obvious example is the resonances shown in figure 2(a). For the CI calculations, the lowest resonance state in the photon energy range shown in figure 2(a) is $(-0.721s2s(^1S) + -0.681s2s(^3S))2p^3(^4S^o)^4S^o$ which is located at 40.0754 Ryd, whereas for the *R*-matrix calculations it is changed to $1s2s(^3S)2p^3(^2D^o)^4D^o$ which is located at 39.9247 Ryd. The interchange of the sequence of states is caused by different CI effects within the continuum. The CI effects in the continuum region with the $^4D^o$ state are much stronger than with the $^4S^o$ state. As a result, the energy of the $^4D^o$ state is decreased so much that it is smaller than that of the $^4S^o$ state after taking account of the interaction between the 1s–2p excited states and continuum ones.

In the above, we discussed the resonance energies and oscillator strengths of the K-shell 1s–2p excitations of O IV ions. As a matter of fact, we have also obtained radiative data for

Table 5. Comparison of the present calculated energies (in Ryd) of the lower (E_l) and upper (E_u) states (relative to the ground state) and transition energies (in Ryd) for the 1s–2p transitions from the low-lying states of O IV. The number of transitions is the same as in table 3.

	CIV3			*R*-matrix		
No	E_l	E_u	ΔE	E_l	E_u	E_r
1	0.0000	40.1739	40.1739	0.0000	39.9848	39.9848
2	0.0000	40.2145	40.2145	0.0000	40.0787	40.0787
3	0.0000	40.4257	40.4257	0.0000	40.2224	40.2224
4	0.6464	40.7533	40.1069	0.6440	40.5331	39.8891
5	0.6464	40.7218	40.0754	0.6440	40.5687	39.9247
6	0.6464	41.0283	40.3819	0.6440	40.7839	39.9247
7	0.6464	41.6384	40.9920	0.6440	41.3432	40.6992
8	1.1684	41.2691	40.1017	1.1568	41.0905	39.9337
9	1.1684	41.5273	40.3589	1.1568	41.3435	40.1867
10	1.1684	41.6703	40.5019	1.1568	41.4368	40.2800
11	1.1684	41.9325	40.7641	1.1568	41.6979	40.5411
12	1.5232	41.4884	39.9652	1.5045	41.3436	39.8391
13	1.5232	41.9137	40.3905	1.5045	41.6980	40.1935
14	1.6676	41.2582	39.5906	1.6508	41.0901	39.4393
15	1.6676	41.5331	39.8655	1.6508	41.3432	39.6924
16	1.6676	41.6474	39.9798	1.6508	41.4365	39.7857
17	1.6676	41.9384	40.2708	1.6508	41.6976	40.0468
18	1.6676	41.9117	40.2441	1.6508	41.7501	40.0993
19	2.1220	42.2457	40.1237	2.1006	41.9932	39.8926
20	2.3469	42.5427	40.1958	2.3222	42.3219	39.9997
21	2.3469	42.6280	40.2811	2.3222	42.4360	40.1138
22	2.6694	42.5868	39.9174	2.6372	42.3219	39.6847
23	2.6694	42.6695	40.0001	2.6372	42.4361	39.7989
24	2.6694	43.1705	40.5011	2.6372	42.8520	40.2148

the valence-shell excited states. As examples, table 6 shows our results as well as the Breit–Pauli results obtained by Tachiev and Froese Fischer [6]. They applied systematic, large-scale methods to obtain wavefunction expansions from orbital sets of increasing size and therefore they obtained accurate results. It can be seen that good agreement is found between the two theoretical results.

Now, let us turn our attention to the autoionization widths of the 1s–2p excited states of O IV displayed in table 3. In one of our previous papers [20], we studied the autoionization widths of the 1s–2p excited states of O III ions. Generally speaking, the autoionization width decreases with the higher ionization stage. For example, the biggest width for O III ions is 177 meV for the $1s2s(^1S)2p^4(^1D)^1D$ term among the low-lying K-shell excited states, while for O IV ions the biggest width is 140.1 meV for the $1s2s^22p^2\ ^2D$ term, a value about 37 meV smaller than the corresponding value for O III. Similarly, the smallest width for O III ions is 56 meV for the $1s2s^22p^3\ ^3S^o$ term, while for O IV ions the smallest width is 19 meV for the $(-0.721s2s(^1S) - 0.681s2s(^3S))2p^3(^4S^o)^4S^o$ term. As a result, the average of the autoionization width for O IV is a little smaller than that for O III ions.

The results in [20] have shown that, under typical oxygen plasma conditions, for example, at a temperature of 10 eV and a mass density of 0.0016 g cm^{-3}, the autoionization widths of the 1s–2p excited states are larger than the Doppler and Stark widths. This is also true for O IV ions. To gain a quantitative understanding, we evaluate the widths caused by the Doppler and Stark broadening mechanisms. The Doppler full width at half maximum (FWHM) can be

Table 6. Comparison of the present calculated energies (in Ryd) of the lower (E_l) and upper (E_u) states (relative to the ground state), transition energies (ΔE) (in Ryd) and oscillator strengths of some valence-shell transitions of the O IV ion with the Breit–Pauli results obtained by Tachiev and Froese Fischer [6].

	This work					Tachiev and Froese Fischer [6]				
Transition	E_l	E_u	ΔE	f_l	f_v	E_l	E_u	ΔE	f_l	f_v
$2s^2 3p\ ^2P^o$–$2s^2 3d\ ^2D$	3.5415	3.8134	0.2719	0.3020	0.2902	3.5567	3.8228	0.2761	0.2913	0.2916
$2s^2 3s\ ^2S$–$2s^2 3p\ ^2P^o$	3.2442	3.5415	0.2972	0.5588	0.5681	3.2575	3.5567	0.2992	0.5454	0.5435
$2s2p^2\ ^2P$–$2p^3\ ^2D^o$	1.6676	2.3469	0.6793	0.1147	0.1092	1.6458	2.3261	0.6803	0.1155	0.1144
$2s2p^2\ ^2P$–$2p^3\ ^2P^o$	1.6676	2.6694	1.0018	0.1698	0.1664	1.6458	2.6362	1.0905	0.1669	0.1666
$2s2p^2\ ^2S$–$2p^3\ ^2P^o$	1.5232	2.6694	1.1462	0.1153	0.1113	1.4989	2.6362	1.1373	0.1168	0.1155
$2s^2 2p\ ^2P^o$–$2s2p^2\ ^2D$	0.0000	1.1684	1.1684	0.1115	0.1070	0.0000	1.1565	1.1565	0.1104	0.1108
$2s2p^2\ ^2D$–$2p^3\ ^2D^o$	1.1684	2.3469	1.1785	0.1323	0.1278	1.1565	2.3261	1.1697	0.1316	0.1313
$2s2p^2\ ^4P$–$2p^3\ ^4S^o$	0.6464	2.1220	1.4756	0.1245	0.1226	0.6513	2.1100	1.4588	0.1209	0.1258
$2s2p^2\ ^2D$–$2p^3\ ^2P^o$	1.1684	2.6694	1.5011	0.1001	0.0982	1.1565	2.6362	1.4798	0.0975	0.0973
$2s^2 2p\ ^2P^o$–$2s2p^2\ ^2S$	0.0000	1.5232	1.5232	0.0681	0.0673	0.0000	1.4989	1.4989	0.0661	0.0659
$2s^2 2p\ ^2P^o$–$2s2p^2\ ^2P$	0.0000	1.6676	1.6676	0.3402	0.3412	0.0000	1.6458	1.6458	0.3321	0.3313
$2s2p^2\ ^2D$–$2s^2 3p\ ^2P^o$	1.1684	3.5415	2.3731	0.0058	0.0076	1.1565	3.5567	2.4003	0.0064	0.0063
$2s^2 2p\ ^2P^o$–$2s^2 3s\ ^2S$	0.0000	3.2442	3.2442	0.0306	0.0313	0.0000	3.2575	3.2575	0.0314	0.0314
$2s2p^2\ ^4P$–$2s2p3s\ ^4P^o$	0.6464	3.9899	3.3435	0.1130	0.1091	0.6513	4.0007	3.3485	0.1131	0.1126
$2s^2 2p\ ^2P^o$–$2s^2 3d\ ^2D$	0.0000	3.8134	3.8134	0.5038	0.4942	0.0000	3.8228	3.8228	0.5013	0.5017

obtained from the following expression [25]:

$$\Gamma(\text{FWHM}) = 7.716 \times 10^{-5}(kT/A)^{1/2}(h\nu_0), \tag{12}$$

where A is the atomic weight of the ion in grams and the units of kT, $h\nu_0$ and Γ are eV. The transition energies of the 1s–2p transitions are located at about 40 Ryd = 544 eV, therefore the Doppler FWHM is about 0.04 eV. This value is, basically, the same as the O III ions under the same condition. Similarly, the Stark FWHM can be estimated to be 0.03 eV. This value was obtained from the semi-empirical method [26] according to the following formula:

$$w = N_e \frac{8\pi}{3}\frac{\hbar^2}{m^2}\left(\frac{2m}{\pi kT}\right)^{1/2}\frac{\pi}{\sqrt{3}}\left(0.9 - \frac{1.1}{Z}\right)\sum_{j=i,f}\left(\frac{3n_j}{2Z}\right)^2(n^2 - l_j^2 - l_j - 1) \tag{13}$$

where N_e and T are the electron density and electron temperature, respectively, $\hbar = h/2\pi$, h is the Planck constant, m is the mass of the electron, $Z-1$ is the ionic charge, $n_i(l_i)$ and $n_f(l_f)$ are the effective principal quantum numbers (the orbital angular momentum quantum numbers) of the lower and upper energy levels of the transition, respectively. From these analyses, one can conclude that the autoionization widths are larger than Doppler and Stark FWHM. This kind of broadening will have a large effect in calculating the K-shell spectroscopy of the O IV ions and oxygen plasma.

In summary, the excitation energies and oscillator strengths of the 1s–2p transitions from the terms belonging to the configurations $2s^2 2p$, $2s2p^2$ and $2p^3$ of O IV ions are investigated by two methods: the CI scheme and a close-coupling scheme implemented by the R-matrix method. Rather good agreement is found between the length and velocity forms of the oscillator strengths obtained by the R-matrix method. They also agree well with the length form obtained by the CI scheme for the strong transitions. However, the excitation energies obtained by the R-matrix method are systematically lower than the results obtained by the CI scheme by 0.1–0.2 Ryd. The differences between the two methods should be attributed to the interaction between the K-shell excited states and continuum states. This kind of interaction can also

produce redistribution of the oscillator strengths. The autoionization widths of these 1s–2p excited states are determined from the photoionization cross sections. We hope that these results will be useful in future experiments on the inner-shell photoionization and absorption spectra of the oxygen plasmas.

Acknowledgments

This work was supported by the National Science Fund for distinguished young scholars under grant no 10025416, by the National Natural Science Foundation of China under grant no 19974075, by the National High-Tech ICF Committee in China, and also by the China Research Association of Atomic and Molecular Data.

References

[1] Fernley J A, Hibbert A, Kingston A E and Seaton M J 1999 *J. Phys. B: At. Mol. Opt. Phys.* **32** 5507
[2] Seaton M J 1987 *J. Phys. B: At. Mol. Phys.* **20** 6363
[3] The Opacity Project Team 1995 *The Opacity Project* vol 1 (Bristol: Institute of Physics Publishing)
[4] Berrington K A, Eissner W B and Norrington P H 1995 *Comput. Phys. Commun.* **92** 290
[5] Nahar S N 1998 *Phys. Rev.* A **58** 3766
[6] Tachiev G and Froese Fischer C 2001 *J. Phys. B: At. Mol. Opt. Phys.* **33** 2419
[7] Saha H P 1994 *Phys. Rev.* A **49** 894
[8] Menzel A, Benzaid S, Krause M O and Caldwell C D 1996 *Phys. Rev.* A **54** R991
[9] Gorczyca T W and McLaughlin B M 2000 *J. Phys. B: At. Mol. Opt. Phys.* **33** L859
[10] Stolte W C, Samson J A R, Hemmers O, Hansen D, Whitfield S B and Lindle D W 1997 *J. Phys. B: At. Mol. Opt. Phys.* **30** 4489
[11] Pradhan A K 2000 *Astrophys. J. Lett.* **545** L165
[12] Lee J C, Ogle P M, Canizares C R, Marshall H L, Schulz N S, Morales R, Fabian A C and Iwasawa K 2001 *Astrophys. J. Lett.* **554** L13
[13] Abdallah J Jr and Clark R E H 1991 *J. Appl. Phys.* **69** 23
[14] Iglesias C A, Chen M H, McWilliams D L, Nash J K and Rogers F J 1995 *J. Quant. Spectrosc. Radiat. Transfer* **54** 185
[15] Zeng J, Jin F, Yuan J, Lu Q and Sun Y 2000 *Phys. Rev.* E **62** 7251
[16] Zeng J, Jin F and Yuan J 2001 *Chin. Phys. Lett.* **18** 924
[17] Zeng J, Yuan J and Lu Q 2001 *Phys. Rev.* E **64** 066412
[18] Hibbert A 1975 *Comput. Phys. Commun.* **9** 141
[19] Zeng J, Yuan J, Zhao Z and Lu Q 2000 *Eur. Phys. J.* D **11** 167
[20] Zeng J, Yuan J and Lu Q 2001 *J. Phys. B: At. Mol. Opt. Phys.* **34** 2823
[21] Burke P G, Hibbert A and Robb W D 1971 *J. Phys. B: At. Mol. Phys.* **4** 153
[22] Zeng J, Yuan J and Lu Q 2000 *Phys. Rev.* A **62** 022713
Zeng J, Yuan J and Lu Q 2001 *Phys. Rev.* A **64** 042704
[23] Clementi E and Roetti C 1974 *At. Data Nucl. Data Tables* **14** 177
[24] Moore C E (ed) 1970 *Atomic Energy Levels (NBS Title Series no I)* (Washington, DC: US Govt Printing Office) p 45
[25] Cowan R D 1981 *Theory of Atomic Spectra* (Berkeley, CA: University of California Press)
[26] Dimitrijevic M S and Konjevic N 1987 *Astron. Astrophys.* **172** 345